Doping effects in the coupled, two-leg spin ladder BiCu$_2$PO$_6$

B Koteswararao[1], A V Mahajan[1], L K Alexander[2] and J Bobroff[2]

[1] Department of Physics, Indian Institute of Technology Bombay, Mumbai 400076, India
[2] Laboratoire de Physique des Solids, Université Paris-Sud, UMR 8502 CNRS,
91405 Orsay Cedex, France

Abstract
We report preparation, x-ray diffraction, magnetic susceptibility $\chi(T)$ and heat capacity $C_p(T)$ measurements on undoped samples as well as samples with Zn-doped ($S = 0$) at the Cu site BiCu$_{2(1-x)}$Zn$_{2x}$PO$_6$, Ni-doped ($S = 1$) at the Cu site BiCu$_{2(1-y)}$Ni$_{2y}$PO$_6$, and Ca doped (holes) at the Bi site Bi$_{1-z}$Ca$_z$Cu$_2$PO$_6$ in the coupled two-leg spin ladder system BiCu$_2$PO$_6$. While, Zn shows complete solid solubility, Ni could be doped to about 20% and Ca to about 15%. Magnetization and heat capacity data in the undoped compound point towards the existence of frustration effects. In all the samples, the $\chi(T)$ at low temperature increases with doping content. The Zn-induced susceptibility is smaller than that due to effective $S = 1/2$ moments, possibly due to frustrating next-nearest-neighbor interactions along the leg. For Zn content $x > 0.01$, $\chi(T)$ deviates from the Curie law at low temperatures. The magnetic specific heat data $C_m(T)$ for the Zn-doped samples show weak anomalies at low temperature, in agreement with the $\chi(T)$ behavior. The anomalies are suggestive of spin freezing at low-T. In contrast, prominent effects are observed in $\chi(T)$ and $C_m(T)$ on Ni-doped samples. The zero-field-cooled (ZFC) and field-cooled (FC) $\chi(T)$ data are different from each other at low temperature, unlike that for Zn-doped samples, clearly indicating a transition to a spin-glass-like phase. No anomalies were found in Ca- or Pb-doped samples.

(Some figures in this article are in colour only in the electronic version)

1. Introduction

Currently, there is great interest in the magnetic properties of pure and doped low-dimensional Heisenberg antiferromagnetic (HAF) and frustrated spin systems. Exotic ground states, such as the valence bond solid (VBS) state in Haldane chains, spin-dimers, and spin-Peierls systems [1], or the resonating valence bond (RVB) state in chain, ladder [2] or planar systems [3, 4], have been investigated. A lot of experimental and theoretical work has been done on the effect of non-magnetic Zn^{2+}($S = 0$) and magnetic Ni^{2+} ($S = 1$) impurities on Cu-based systems. When Cu^{2+} ions in hole-doped, metallic CuO$_2$ planes in YBa$_2$Cu$_3$O$_{6+\delta}$ are substituted with Zn^{2+}, nuclear magnetic resonance (NMR) experiments [5] revealed that local magnetic moments are induced on neighboring Cu sites. Further NMR studies [6] investigated the effect of impurities on the magnetic correlations and showed that each vacancy causes a strong antiferromagnetic polarization around its immediate vicinity [7]. This phenomenon was also observed in Ni-doped

square lattices [8]. Similar behavior was also found in Haldane chains [9] and ladders [10, 11].

In the case of $S = \frac{1}{2}$, even-leg spin ladders (which have a spin-gap), a transition from the spin-liquid ground state to an ordered state across a quantum critical point (QCP) can occur as a function of some tuning parameter such as the inter-ladder coupling [4]. Additionally, non-magnetic impurities have been found to induce disordered magnetism or magnetic long-range-order (LRO) in a prototypical two-leg ladder such as SrCu$_2$O$_3$. [12, 13] In SrCu$_2$O$_3$, the exchange interaction along the leg (J_1/k_B) was found to be 1900 K. The ratio of the rung exchange to leg exchange J_2/J_1 and the spin-gap (Δ/k_B) were found to be 0.5 and 450 K, respectively, with only a weak inter-ladder interaction [14]. In this spin gapped system, even a small amount of disorder by introduction of non-magnetic Zn^{2+}($S = 0$) impurities at the Cu^{2+} site induces long-range AF ordering at the Neel temperature T_N, ranging from 3 to 8 K for $0.01 \leqslant x \leqslant 0.08$ [13]. The specific heat measurements above T_N for $x = 0.02$ and 0.04 also confirmed

the gapless antiferromagnetic state from its linear variation with temperature, which should be observed in gapless systems such as uniform spin chains [15]. Similar AF ordering was also found in Ni-doped $SrCu_2O_3$ from NMR experiments [10]. On the other hand, in the systems which are beyond the QCP, i.e., on the LRO side of the phase diagram, such as the 2D square planar La_2CuO_4, doping with Zn leads to a reduction of T_N [16]. In contrast, the physics of defect-induced moments in geometrically frustrated spin systems, such as kagome [17, 18], hyper-kagome systems [19], etc is quite different from non-frustrated spin systems. These interesting results inspired us to look for new quantum spin systems and investigate the impurity effects in them.

Recently, we have reported the magnetic susceptibility and the specific heat of a new spin ladder system, $BiCu_2PO_6$, in which the exchange interaction along the leg J_1/k_B was found to be 80 K and the ratio of the rung to leg exchange coupling J_2/J_1 to be nearly 1 [20]. From these exchange couplings and magnetic specific heat, we estimated a spin-gap (Δ/k_B) of 34 K, which is in good agreement with the previously reported value of 33 K [21]. The first-principles band structure and magnetic susceptibility analysis [20] suggested a strong inter-ladder coupling $J_3/J_1 \sim 0.75$ in the bc-plane, and a next-nearest-neighbor (*nnn*) exchange interaction along the leg $J_4/J_1 \sim 0.34$. While we are not aware of any calculations of the QCP for 2D coupled two-leg ladders with a frustrating *nnn* interaction along the leg, $J_3/J_1 \sim 0.75$ would seem to be very large and presumably close to a QCP. Perturbing this ground state by doping with non-magnetic or magnetic impurities can reveal important information about the nature of the system.

Furthermore in an earlier paper [22], we have used local probe measurements (nuclear magnetic resonance NMR and muon spin resonance μSR) to probe impurity (Zn and Ni) effects in the $BiCu_2PO_6$ spin ladder. We have shown the appearance of impurity-induced moments leading eventually to spin freezing at low temperatures. We now report bulk (magnetic susceptibility and heat capacity) measurements on the pure, and doped (homovalent Zn, Ni at Cu site and heterovalent Pb, Ca at Bi site) HAF spin ladder $BiCu_2PO_6$ i.e. $Bi(Cu_{1-x}Zn_x)_2PO_6$, $Bi(Cu_{1-y}Ni_y)_2PO_6$ and $Bi_{1-z}Ca_zCu_2PO_6$. While such measurements validate the sample quality, and surely constitute the first steps to investigate the gross properties of a system such as the occurrence of a spin-gap, phase transitions, etc, they also enable us to reach conclusions about details such as the applicability (or lack thereof) of theoretical models (isolated spin ladder, Majumdar–Ghosh chain, dimer model, etc) and the value of the impurity-induced magnetic moment. These are useful inputs to theorists to refine and improve their theoretical models. Our magnetic susceptibility measurements on Zn-doped $BiCu_2PO_6$ evidence low temperature upturns due to induced magnetic moments. The data also suggest that the Zn-induced moment is smaller than that expected for isolated ladders and is likely related to frustrations present in our system. In the case of Ni doping, a transition to a spin-glass-like disordered state is clearly evident in the susceptibility data. Anomalies were also observed in the heat capacity data. Similar to Zn-doped samples, in Ni-doped samples the induced

moment (combination of the Ni magnetic moment and the neighboring staggered moments) is found to be smaller than that for an isolated $S = 1$ entity. No anomalies were found in the susceptibility or heat capacity data of Ca- or Pb-doped samples.

2. Experimental details

Polycrystalline samples of $BiCu_{2(1-x)}Zn_{2x}PO_6$, $(0 \leqslant x \leqslant 1)$, $BiCu_{2(1-y)}Ni_{2y}PO_6$, $(0 \leqslant y \leqslant 0.2)$, $Bi_{1-z}Pb_zCu_2PO_6$, $(0 \leqslant z \leqslant 0.07)$ and $Bi_{1-z}Ca_zCu_2PO_6$, $(0 \leqslant z \leqslant 0.15)$ were prepared by conventional solid state reaction methods, using Bi_2O_3, CuO, ZnO, NiO, $CaCO_3$ and $(NH_4)_2HPO_4$. Samples were ground, pelletized, and fired at 770 °C for four days with three intermediate grindings. X-ray diffraction measurements were performed using a PANalytical X'pert PRO powder diffractometer. All the above samples were found to be single phase and structural parameters were refined using Fullprof software [23]. Magnetization M was measured as a function applied magnetic field H and temperature T ($2 \leqslant T \leqslant 300$ K) using a SQUID magnetometer and a vibrating sample magnetometer (VSM) of a Physical Property Measurement System (PPMS), both from Quantum Design, Inc. The specific heat C_p measurements were performed as a function of T in the range 1.8–70 K by the relaxation method using the PPMS.

3. Results and analysis

3.1. Crystal structure and lattice parameters

In the crystal structure of $BiCu_2PO_6$ [24], two edge-shared CuO_5 distorted square pyramids, which are built from two different Cu (Cu1 and Cu2) and O (O1 and O2) atoms, respectively, form zigzag two-leg ladders along the crystallographic b-direction. The bond angle and bond length along the leg (Cu1–O1–Cu2) of the ladder are about 112° and 3.2 Å, respectively, and along the rung (Cu1–O2–Cu2) the corresponding values are 92° and 2.8 Å, respectively (see figure 1(a)). The Bi atoms are positioned between the ladders in the bc-plane, as shown in figure 1(b). These planes are separated by PO_4 tetrahedron units. Various exchange couplings (J_1, J_2, J_3, and J_4) between Cu atoms in its bc-plane have been indicated in figure 1(c). Further, various important bond lengths and bond angles are given in table 1.

All the above mentioned samples were found to be single phase from x-ray diffraction (XRD) measurements and Rietveld refinement analysis. The Rietveld refinement pattern for the undoped sample is shown in figure 2(a). The XRD patterns for Zn-doped samples were also indexed based on the orthorhombic space group $Pnma$. The XRD peaks shift towards smaller angles 2θ as the Zn content changes from $x = 0.0$ to 1.0, which is a clear indication of a change in the lattice parameters. The yielded lattice parameters a, b, and c from the refinement are plotted as a function of x in figure 2(c). The lattice parameters of $BiCu_2PO_6$ ($x = 0$) and $BiZn_2PO_6$ ($x = 1$) are in reasonable agreement with previously reported data [24] and the values for intermediate concentrations also smoothly interpolate between the end points. The changes in lattice parameters on Ni, Pb, and Ca doping (not shown here) are somewhat less than that on Zn doping.

Table 1. Various exchange paths and their corresponding bond angles and bond lengths are given for the $BiCu_2PO_6$ structure illustrated in figure 1.

Path	Bond lengths	Bond angles (deg)
Cu1–O1–Cu2 (J_1/k_B)	Cu1–O1 $\sim$ 1.94 Å, Cu2–O1 $\sim$ 1.94 Å	112
Cu1–O2–Cu2 (J_2/k_B)	Cu1–O2 $\sim$ 2.03 Å, Cu2–O2 $\sim$ 2.0 Å	92
Cu1–Bi–Cu2 (J_3/k_B)	Cu1–Bi $\sim$ 3.24 Å, Cu2–Bi $\sim$ 3.38 Å	95.6
Cu1–O2–P–O2–Cu1 (J_4/k_B)	Cu1–O2–P $\sim$ 3.3 Å, P–O2–Cu1 $\sim$ 3.3 Å	Cu1–O2–P $\sim$ 137, O2–P–O2 $\sim$ 109.8, P–O2–Cu1 $\sim$ 137
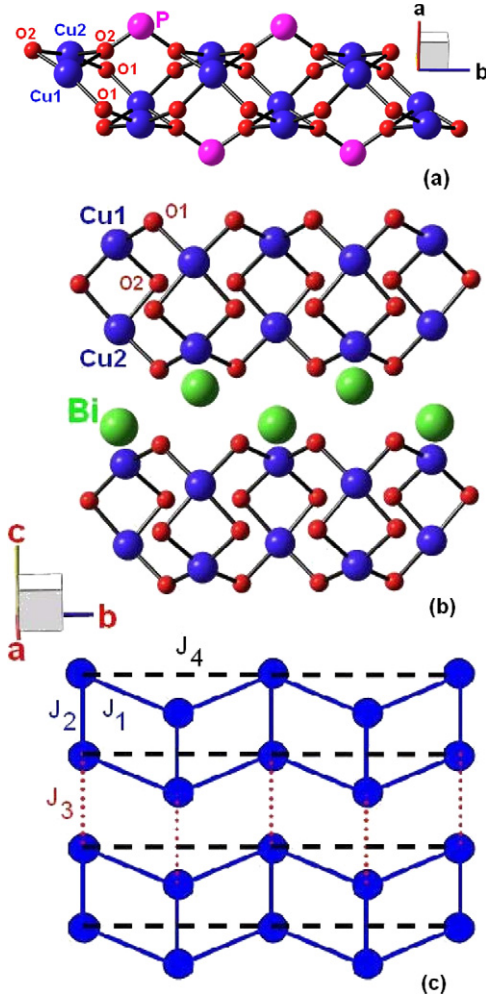
Figure 1. (a) The two-leg spin ladder along the *b*-direction is shown. The leg and rung exchange couplings between Cu1 and Cu2 are mediated by O1 and O2 atoms, respectively, and the next nearest neighbor coupling along the leg is mediated by O–P–O atoms. (b) The crystallographic *bc*-plane of $BiCu_2PO_6$ is also shown, and it can be seen that coupled two-leg zigzag ladders are formed by Cu (blue) and O (red) atoms while Bi (green) atoms are positioned in between. The various major exchange interactions between the Cu atoms are shown in the schematic (c).

## 4. Magnetic susceptibility and heat capacity

4.1. Undoped BiCu₂PO₆

The temperature dependence of bulk magnetic susceptibility $\chi(T) = M/H$ for $BiCu_2PO_6$ is shown in figure 3. The $\chi(T)$ shows a broad maximum at about 56 K, indicative of a low-dimensional magnetic system, thereafter decreasing steeply

with decreasing temperature. This is indicative of a gap in the spin excitation spectrum in agreement with the 2-leg ladder geometry suggested by the structure. A small upturn appears below 7 K, likely due to extrinsic paramagnetic impurities and/or natural chain breaks in our polycrystalline samples. We first fit the low temperature part of $\chi(T)$ below 15 K to the equation [25]

$$\chi(T) = \chi_0 + \frac{C}{(T-\theta)} + \frac{A}{\sqrt{T}} \exp\left(-\frac{\Delta}{k_B T}\right). \quad (1)$$

This yields the parameters $\chi_0 = (4.4 \pm 0.2) \times 10^{-4}$ cm³ mol⁻¹ Cu, $C = (3.6 \pm 0.2) \times 10^{-4}$ cm³ K mol⁻¹ Cu, $\theta \sim 0$ K, $A = \frac{Ng^2\mu_B^2}{2k_B\sqrt{\pi(\frac{\gamma}{k_B})}} = (2.6 \pm 0.1) \times 10^{-2}$ and the spin-gap $\Delta/k_B = (45 \pm 3)$ K. Here k_B is the Boltzmann constant, N is the Avogadro number, g is the Landé *g*-factor (fixed to 2.1, a typical value in cuprates), and γ is the curvature of magnon dispersion at the band minimum. The temperature independent susceptibility χ_0 is the sum of the core diamagnetic susceptibility χ_{core}, the Van Vleck susceptibility χ_{vv} and a residual susceptibility χ_{res} (this will be explained shortly). χ_{core} is calculated [26] to be -0.6×10^{-4} cm³ mol⁻¹ Cu. Our recent NMR results [27] have shown that the ^{31}P NMR shift (and hence the spin susceptibility) falls exponentially at low-*T* due to the gap, there remains a non-zero NMR shift as $T \rightarrow 0$. This amounts to a residual spin susceptibility $\chi_{res} = 1.4 \times 10^{-4}$ cm³ mol⁻¹ Cu. Using this value of χ_{res} we get $\chi_{vv} = 3.6 \times 10^{-4}$ cm³ mol⁻¹ Cu which is somewhat higher than χ_{vv} of other cuprates. The Curie constant corresponds to about 0.1% of isolated spin-$\frac{1}{2}$ impurities. In a latter section, we analyze the impurity-induced susceptibility in greater detail. The ratio γ/Δ was also found from the fit. However, due to the small amount of data at low-*T*, the result was found to be dependent on the *T*-range used for the fit and is therefore considered unreliable.

In order to gain further insight into the magnetic interactions present in this system, we now attempt to fit the susceptibility data in the full temperature range for undoped $BiCu_2PO_6$. Note that while the measured susceptibility has a low-*T* Curie term (albeit small) the spin susceptibility obtained via the ^{31}P NMR shift measurements ($\chi_{NMR}(T)$, detailed in a separate paper [27]) is intrinsic and has no Curie term. The NMR shift $K(T)$ is proportional to the intrinsic spin susceptibility $\chi_{NMR}(T)$ via the equation $N_A\mu_B K(T) = H_{hf}\chi_{NMR}(T)$, where H_{hf} is the hyperfine coupling constant. As a result, small amounts of extrinsic impurities do not affect the NMR line position and the measured $K(T)$ reflects the intrinsic behavior. Furthermore, for dilute concentrations of intrinsic impurities (substitutions), the NMR mainline position
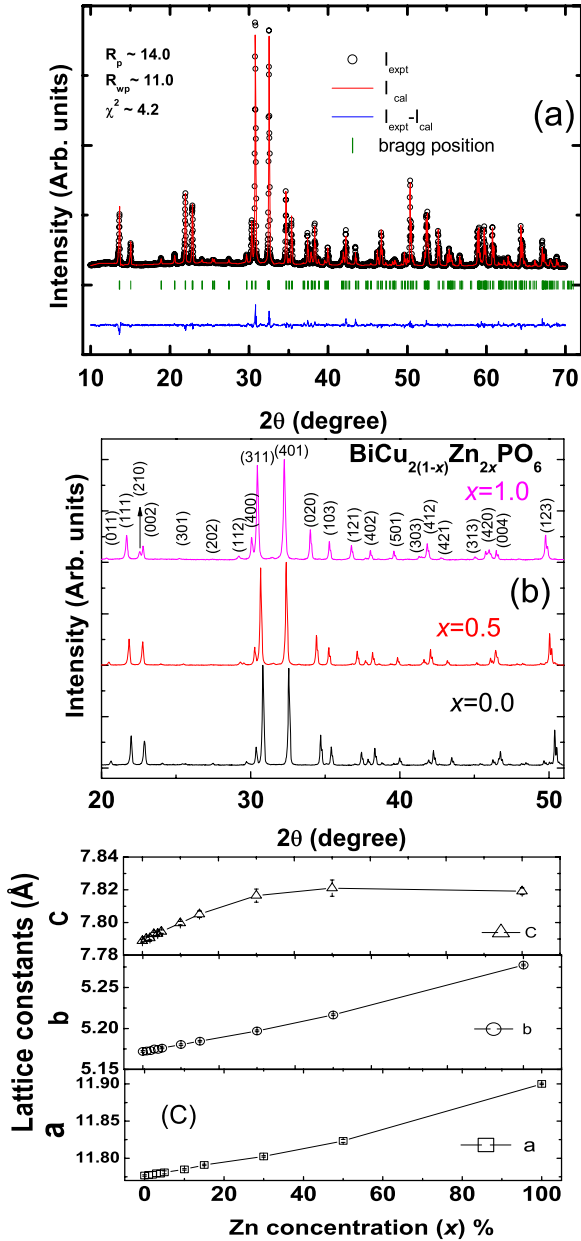
Figure 2. The x-ray diffraction pattern of $BiCu_2PO_6$ is shown along with the Rietveld refinement. The black open circles indicate the experimental XRD data, the solid red line is calculated based on the refinement, green vertical short lines are the Bragg positions and the blue line is the difference of measured and calculated data. The refinement parameters are $R_p = 14.0$, $R_{wp} = 11.0$ and $\chi^2 = 4.2$. (b) The XRD patterns of $BiCu_{2(1-x)}Zn_{2x}PO_6$ ($x = 0.0$, 0.5 and 1.0) with hkl-indices are shown. (c) The lattice constants a, b, and c as a function of Zn doping content (x) are shown in (c).

reflects the intrinsic susceptibility of sites which are far away from the impurity. Therefore the Curie-like terms seen in the bulk susceptibility of impurity-substituted samples, which might contain both intrinsic and extrinsic effects, do not affect the NMR line shift, while the intrinsic impurities give rise to a broadening and possibly additional, weak, satellite lines. We have, therefore, used $\chi_{NMR}(T)$ to carry out the analysis following equation (2) below [28]. This kind of equation has been used in the past to determine the strength of inter-dimer,
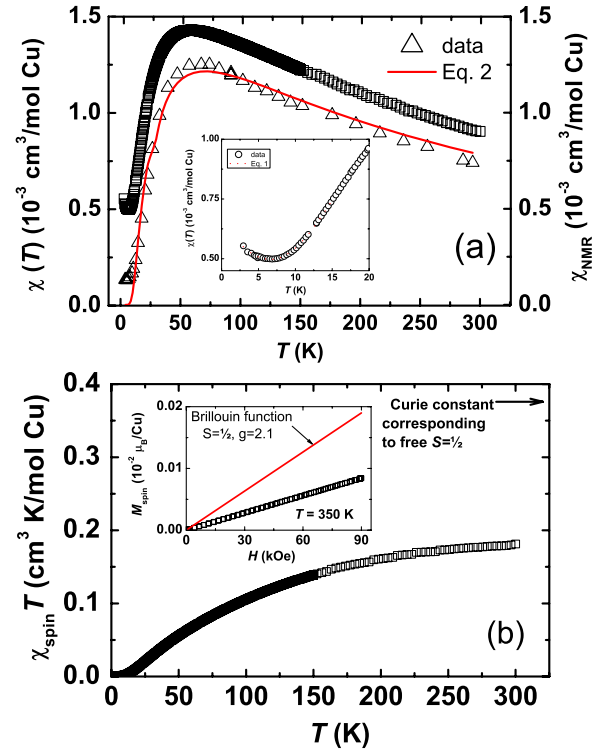
Figure 3. (a) Magnetic susceptibility $\chi(T) = (M/H)$ versus temperature T (open squares) for $BiCu_2PO_6$ in an applied field of 5000 Oe. Also plotted is $\chi_{NMR}(T)$ (open triangles). The solid line is a fit to equation (2) of $\chi_{NMR}(T)$. As shown in the inset (a), the dashed line is a fit to the equation (1), as explained in the text. In (b), $\chi_{spin}T$ is plotted as a function of T and the inset shows the magnetization (M) as a function of magnetic field (H) up to 90 kOe and a comparison with the Brillouin function at 350 K. The arrow mark indicates the value corresponding to the Curie constant (C) for free spin-$\frac{1}{2}$.

inter-chain, and inter-ladder interactions in the corresponding systems (non-frustrated) such as $SrCu_2O_3$ [14], CaV_2O_5 [28], $Sr_3Cr_2O_8$ [29] etc

$$\chi_{NMR}(T) = \frac{Ng^2\mu_B^2}{J_1}\left(\frac{\chi_{ladder}^*(J_1, J_2, T)}{1 + \lambda\chi_{ladder}^*(J_1, J_2, T)}\right). \quad (2)$$

Here, $\chi_{ladder}^*(J_1, J_2, T) = \frac{J_1}{Ng^2\mu_B^2}\chi_{ladder}(T)$ (with $\chi_{ladder}(T)$ being the isolated ladder susceptibility [28]), while $\lambda(= 2(z_{eff} - z_0))$ accounts for the intersystem exchange coupling. The fitting parameters depend somewhat on the T-range used for the fit. The obtained values for the leg and rung coupling are about $J_1/k_B \sim 80$ K and $J_2/k_B = 78$ K. Also, λ is found to be in the range 8–10. Given that z_0, the magnetic coordination number, in the case of the isolated ladder is 3, we get the effective magnetic coordination number $z_{eff} \sim 7$–8. Using this, and our experimental value of $\chi^{max} = \chi_{NMR}^{max} = 1.25 \times 10^{-3}$ cm^3 mol^{-1} Cu, we get $\frac{\chi^{max}J^{max}z_{eff}}{Ng^2\mu_B^2} = 0.42$–0.48, which lies a little above the universal curve (for non-frustrated bipartite AF spin lattices) given by Johnston (see figure 4 of [14]). Further, Johnston [14] made the observation that $\frac{\chi^{max}J^{max}z_{eff}}{Ng^2\mu_B^2}$ lies above the universal curve for highly frustrated systems, such as the triangular system and other cluster

systems where the frustrating interaction is equal to the other interaction. One might, therefore, naively conclude that $BiCu_2PO_6$ might be only moderately frustrated. Numerical computations for a coupled ladder system (with frustrations) are not available, since a technique like quantum Monte Carlo (QMC) simulations can not treat both effects at the same time. We have, in an earlier paper [22], made an attempt to extract the most salient features of our system by performing QMC simulations, by including the inter-ladder coupling as also determining the effects of impurity substitutions in such a system. This has enabled us to improve our understanding of impurity-induced order in ladder systems, in general.

The plot of $\chi_{\mathrm{spin}}T (= (\chi - \chi_{\mathrm{core}} - \chi_{vv})T)$ versus T for undoped $BiCu_2PO_6$ is shown in figure 3(b). Even at 300 K, which is nearly four times the value of J^{max}/k_B, the value of $\chi_{\mathrm{spin}}T$ is about 0.185 and smaller than 0.375, which is the value of $\chi_{\mathrm{spin}}T$ in the paramagnetic limit. This suggests that the system is not in the paramagnetic limit even at 300 K. As a further illustration, we show the spin magnetization $M_{\mathrm{spin}}(H)$ as a function of applied field at $T = 350$ K, with the comparison of Brillouin function for $S = \frac{1}{2}$ and $g = 2.1$ in the inset of figure 3(b). Clearly, the data are well below the Brillouin function curve. These results suggest that AF and frustrating interactions are present even at $T = 350$ K.

Theoretically, a coupled two-leg spin ladder system ($J_1 = J_2$) has a quantum critical point (QCP) at about $J_3/J_1 = 0.3$, which separates the spin-gap region from the LRO antiferromagnetic region [4]. Experimentally, however, we have proven that this system has a spin-gap of about 35–40 K. Recent inelastic neutron scattering results on $BiCu_2PO_6$ yield a spin-gap of about 1.5 meV (equivalent to 20 K) [30]. The difference with our results could be due to a wave-vector dependence of the spin-gap affecting the neutron scattering results on powder samples. From theory, it is known that in two-leg ladders the existing spin-gap increases due to frustrating *nnn* interactions [31]. Also, from theoretical DMRG calculations, it is predicted that the three-leg spin ladder (which is gapless) will develop a spin-gap in the case of frustrating *nnn* interactions. The continued presence of the spin-gap state in our system, in spite of the relatively large inter-ladder couplings (predicted from electronic structure calculations [20]), points to the presence of frustrating interactions. It is likely that the next-nearest-neighbor (*nnn*) coupling J_4 is frustrating, and plays a role in sustaining the spin-gap state.

The specific heat $C_p(T)$ of $BiCu_2PO_6$ is shown in figure 4. We have analyzed $C_p(T)$ of $BiZn_2PO_6$, the non-magnetic analog of $BiCu_2PO_6$, using the Debye model [32]. The data could not be fit using a single Debye temperature, probably because of different atoms having different atomic weights. We were able to fit the data to the following formula, which contains a linear combination of two Debye integrals.

$$C_p(T) = 9rNk_B \sum_{i=1,2} C_i \left(\frac{T}{\theta_D^i}\right)^3 \int_0^{x_D^i} \frac{x^4 e^x}{(e^x - 1)^2} \, dx. \quad (3)$$

Here r is the number of atoms per formula unit, θ_D^i is a Debye temperature and $x_D^i = \theta_D^i/T$. The obtained parameters
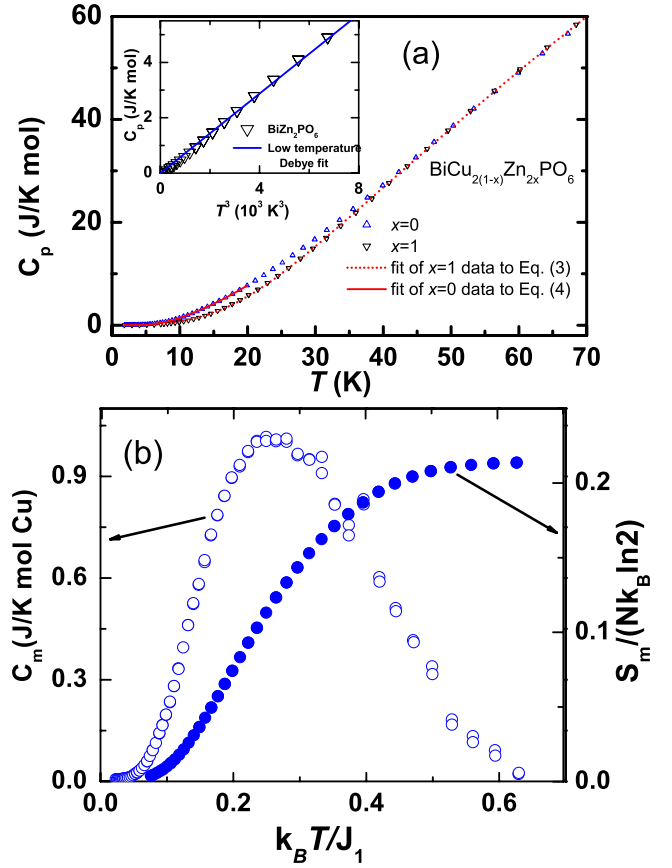

Figure 4. (a) The specific heat C_p as a function of T for $BiCu_2PO_6$ (blue open up-triangles) and $BiZn_2PO_6$ (black open down-triangles) is shown and fitted with the equations mentioned in the text. The inset shows the data of C_p as a function of T^3 for $BiZn_2PO_6$. (b) The magnetic contribution to the specific heat of $BiCu_2PO_6$ (left axis) is plotted versus the normalized temperature k_BT/J_1. Also shown is the magnetic entropy S_M (right axis) versus k_BT/J_1.

are $C_1 = 0.20 \pm 0.01$, $\theta_D^1 = 183 \pm 2$ K, $C_2 = 0.41 \pm 0.01$, and $\theta_D^2 = 456 \pm 6$ K. Further we also fit the $C_p(T)$ of $BiZn_2PO_6$ data to the low-T Debye expression ($\frac{12\pi^4}{5} Nrk_B (\frac{T}{\theta_D})^3$) in the T-range from 2 to 20 K. The yielded θ_D is (325 ± 2) K and is intermediate to θ_D^1 and θ_D^2. In the same T-range, we go ahead and fit the $C_p(T)$ data of $BiCu_2PO_6$ using the following equation:

$$C_p(T) = \frac{12\pi^4}{5} Nrk_B \left(\frac{T}{\theta_D}\right)^3 + \frac{3}{2} Nrk_B \left(\frac{\Delta}{\pi\gamma}\right)^{1/2}$$
$$\times \left(\frac{\Delta}{k_BT}\right)^{3/2} \left[1 + \frac{k_BT}{\Delta} + 0.75 \left(\frac{k_BT}{\Delta}\right)^2\right] \exp\left(\frac{-\Delta}{k_BT}\right). \quad (4)$$

Here the yielded value of $\theta_D = 330 \pm 2$ from the first part is nearly the same as the value of θ_D of $BiZn_2PO_6$. Hence we used $C_p(T)$ of $BiZn_2PO_6$ as the lattice contribution for the $BiCu_2PO_6$ (as mentioned before) and the magnetic part $\frac{C_m(T)}{T}(x = 0.0)$ is plotted in figure 6. Exponential behavior, a broad maximum, and a lack of LRO are the indications of spin-gap systems. The second term is the magnetic specific heat for two-leg spin ladders [28]. A fit of our data to the
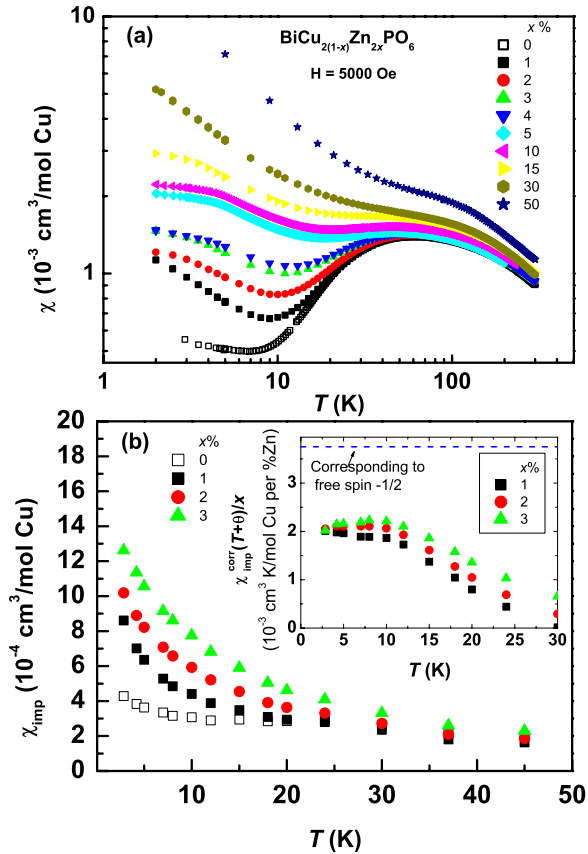
Figure 5. (a) Magnetic susceptibility versus temperature $\chi(T)$ for BiCu$_{2(1-x)}$Zn$_{2x}$PO$_6$, ($0 \leqslant x < 0.5$) in the range 2–300 K, measured in the applied field 5000 Oe. (b) A plot of the non-spin-gap part of the susceptibility χ_{imp} for BiCu$_{2(1-x)}$Zn$_{2x}$PO$_6$ (i.e., only from impurity-induced effects and from extrinsic impurities) is shown as a function of T. The inset shows $\chi_{\text{imp}}^{\text{corr}}(T+\theta)$ per per cent Zn as a function of T. The dashed horizontal line represents the value corresponding to an $S = 1/2$ induced moment per per cent Zn.

above equation yields $\Delta = 43 \pm 2$ K (in good agreement with the 45 K value from low-T susceptibility analysis) and $\gamma/\Delta = 6 \pm 1$. The magnetic entropy S_m is estimated by integrating the data $\frac{C_m(T)}{T}$ versus T. The normalized $S_m(S_m^*)$ is plotted as a function of reduced temperature $T^*(= k_B T/J_1)$ in the inset of figure 6. The value of S_m^* at $T^* = 0.5$ is 0.2, which is 35% of the value of 0.56 for an $S = \frac{1}{2}$ uniform chain which is non-frustrated [33]. The quenching of magnetic entropy at low temperature is a hallmark of frustrated spin systems.

4.2. Zn-doped BiCu$_2$PO$_6$

The magnetic susceptibilities of Zn^{2+} ($S = 0$) doped at the Cu^{2+} site in the BiCu$_2$PO$_6$ samples i.e., BiCu$_{2(1-x)}$Zn$_{2x}$PO$_6$, ($0 \leqslant x \leqslant 0.5$), were measured in an applied field of 5000 Oe, as shown in figure 5(a). The susceptibility at low temperatures increases with the doping concentration x. Introduction of Zn^{2+} at Cu^{2+} in the ladder creates spin vacancies, which are expected to induce localized magnetic moments on the neighboring Cu sites. The effect of induced moments has certainly been observed by us in NMR and μSR measurements [22]. For the case of an isolated $S = 1/2$ HAF 2-leg ladder, the effective magnetic moment per vacancy is
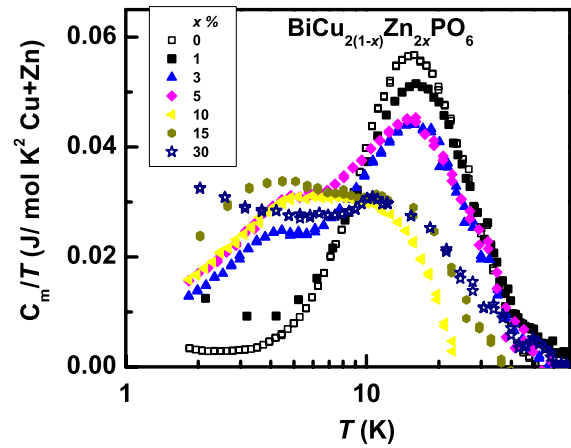
Figure 6. Magnetic specific heat divided by temperature $C_m(T)/T$ versus T for BiCu$_{2(1-x)}$Zn$_{2x}$PO$_6$, ($0 \leqslant x \leqslant 0.3$) in the range 2–50 K.

expected to be exactly that due to an $S = 1/2$ entity. For $x \geqslant 0.02$, it is clear that the low-T ($T < 6$ K) behavior is not Curie-like (there is a deviation from linearity in the log–log plot of figure 5(a)). We analyze the low-T behavior in the susceptibility in the following manner. There are both intrinsic (natural defects/chain breaks, impurity-induced effects, spin-gap) and extrinsic (impurity phase) contributions to the susceptibility in all the samples. As argued [27], the spin susceptibility due only to the spin-gap (χ_{NMR}) is obtained from the ^{31}P NMR shift. Next, we subtract χ_{NMR} from the measured susceptibility χ. This yields $\chi_{\text{imp}}(x, T)$, which is the combination of a T-independent part and a T-dependent part due to defects, dopants, and extrinsic impurities and is shown in figure 5(b). As seen, the undoped sample has a weakly T-dependent contribution. We then plot $\chi_{\text{imp}}^{\text{corr}}(T+\theta)$ divided by the Zn concentration, as a function of T, in the inset of figure 5(b). The impurity susceptibility is $\chi_{\text{imp}}^{\text{corr}} = \chi_{\text{imp}}(x) - \chi_{\text{imp}}(x = 0) - \chi_0$, where χ_0 is a T-independent term. Here, θ is taken equal to T_g, which is the temperature below which a frozen magnetic state was evidenced from μSR measurements. For a pure Curie–Weiss behavior, $\chi_{\text{imp}}^{\text{corr}}(T+\theta)$ should be T-independent, giving the value of the Curie constant. Our result is seen to be not quite T-independent (the nature of the data are not much dependent for θ between 0 and T_g). However, χ_{imp} increases linearly with Zn content. Also, it is seen that the impurity-induced susceptibility is smaller (consistent with an effective paramagnetic moment of $S \sim 0.3$) than the case where each Zn induces an effective $S = 1/2$ moment (the dashed line in the inset of figure 5(b)). This might be related to the presence of frustrating interactions in the compound. While the details of ^{31}P NMR measurements in pure and doped BiCu$_2$PO$_6$ are discussed in a separate paper [27], suffice to say at this point that the data are consistent with the nominal Zn/Ni content in the ladder. The position of the broad maximum in $\chi(T)$ does not appear to change with Zn content, as shown in figure 5(a). Surprisingly even for $x = 0.5$, a broad maximum is seen. No difference in the zero-field-cooled (ZFC) and field-cooled (FC) susceptibilities was seen at low-T. However, the deviation from the Curie behavior seems to suggest transition to a new magnetic state. These results are different from

those of $SrCu_2O_3$, in which cusp-like anomalies were found in $\chi(T)$ [13].

Quite generally, the replacement of Cu^{2+} ion with Zn^{2+} in a spin-liquid with a singlet ground state, such as in HAF two-leg spin ladders, induces an effective spin-$\frac{1}{2}$ moment [34]. However, a deviation from the free, spin-$\frac{1}{2}$ moment was predicted in $S = 0$ doped, one-dimensional, dimerized, frustrated (Majumdar–Ghosh) chains [35]. Considering that $BiCu_2PO_6$ can be thought of as consisting, essentially, of coupled Majumdar–Ghosh chains, predictions by Normand and Mila might be valid here. The reduced Curie constants (compared to the $S = 1/2$ value) observed by us in Zn-doped samples might be an evidence of this. However, there may be other explanations. For higher doping concentrations, interaction between the induced moments result in deviations in the $\chi(T)$ from a Curie law. The origin of the disordered magnetic state which has been observed may be connected to random exchange interactions between impurity-induced local magnetic moments on Cu sites on ladders in different *bc*-planes.

In order to better understand the properties of Zn-doped $BiCu_2PO_6$, we have also performed the specific heat $C_p(T)$ measurements for $x \leqslant 0.30$. After subtracting the lattice contribution from the data for the non-magnetic analog $BiZn_2PO_6$, the obtained magnetic contribution C_m/T versus T is plotted in figure 6. Here we found that even for small doping level $x = 0.01$, an upturn is seen at low-T. This is possibly indicative of an onset of magnetic freezing. For higher x, a broad anomaly is seen around 4 K. These suggest the loss of the spin-gap and a freezing of impurity-induced moments. Due to the small magnetic heat capacity and the weak anomaly, we do not have good accuracy in determining the freezing temperature. However, the anomalies in C_m/T versus T are in the same range as found by our μSR measurements on the same samples [22].

4.3. Ni-doped BiCu$_2$PO$_6$

The $\chi(T)$ of $Ni^{2+}(S = 1)$ doped $BiCu_2PO_6$ were measured in the T-range 2 to 300 K and are shown in figure 7(a). At low-T, an enhancement of susceptibility with Ni content (y) was observed and for higher contents ($y \geqslant 0.15$), even the high-T susceptibility increased with y. At low doping levels, we again carried out the analysis as for Zn doping. The plot of $\chi_{imp}^{corr}(T + \theta)$ for Ni-doped samples is shown in figure 7(b). A Ni dopant is expected to give rise to two contributions; (i) a staggered magnetization on the neighboring Cu sites as for the Zn and (ii) the magnetic moment of the Ni itself. While the 'effective' Curie constant induced per per cent of Ni (about 0.006 cm^3 K mol^{-1}) is clearly greater than that for Zn, the value is smaller than that expected for 1 % of paramagnetic $S = 1$ entities. This indicates that the Ni^{2+} impurity moments may be coupled antiferromagnetically with induced moments on neighboring Cu sites. However, it is also possible that there is a ferromagnetic coupling between the Ni and the neighboring Cu. An agreement with our experimental results can be achieved if there is also a frustration related screening which decreases the size of the paramagnetic cloud comprising
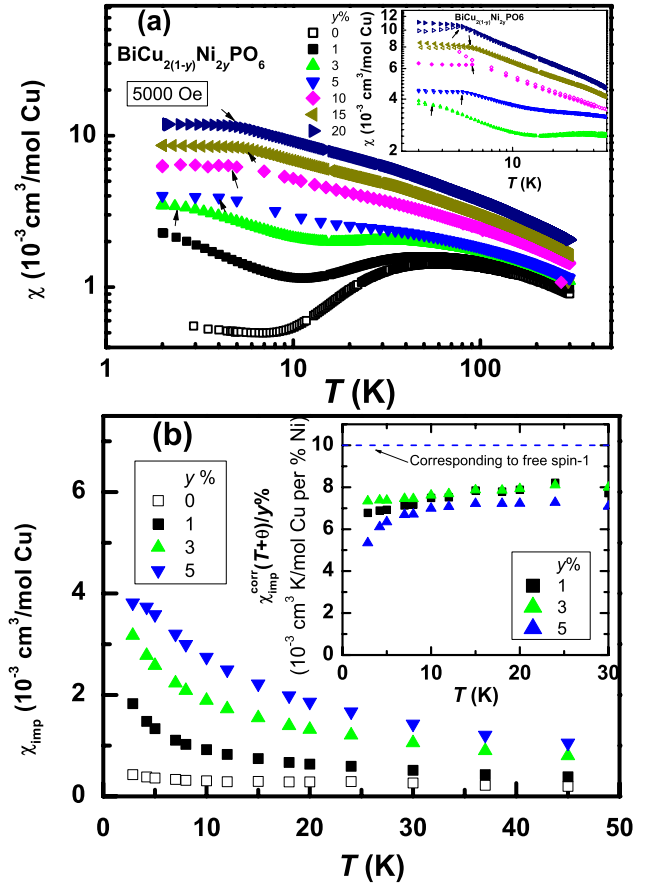
Figure 7. (a) The $\chi(T)$ of $BiCu_{2(1-y)}Ni_{2y}PO_6$ ($0 \leqslant y \leqslant 0.2$), measured in a magnetic field of 5000 Oe and plotted on a log–log scale. The ZFC and FC susceptibility $\chi(T)$ measured in 100 Oe is shown in the inset. The arrow marks at bifurcation points are indicative of the freezing temperature. (b) A plot of the non-spin-gap part of the susceptibility χ_{imp} for $BiCu_{2(1-x)}Ni_{2x}PO_6$ (i.e., only from impurity-induced effects and from extrinsic impurities) is shown as a function of T. The inset shows $\chi_{imp}^{corr}(T + \theta)$ per per cent Ni as a function of T. The dashed horizontal line represents the value corresponding to an $S = 1$ induced moment per per cent Ni.

of the Ni moment and the induced moments on the neighboring Cu. Similar to Zn-doped samples, at low temperatures $\chi(T)$ deviates significantly from a Curie behavior. In addition, there are differences observed in ZFC and FC $\chi(T)$ data measured in an applied field 100 Oe, as shown in inset of figure 7. Specific heat data are further measured to understand these anomalies. Sharp cusp-like anomalies are found with Ni doping, as shown in figure 8. The temperatures at which these anomalies are present are similar to those in $\chi(T)$ data. The exponential T-dependence and the broad maximum present in the $C_m(T)$ of the undoped composition were lost on Ni doping, indicating a loss of the spin-gap. The cusps in the heat capacity are likely associated with spin freezing (similar features have been noticed in Zn- and Ni-doped $SrCu_2O_3$ [13] and $CuGeO_3$ [36]). Note that the susceptibility or heat capacity anomalies are not sharply defined in our data (in fact, if one looks at C_m versus T, only a broad feature is seen). Keeping this in mind, in our μSR measurements (where the freezing temperature is obtained precisely) on the same samples [22], we observed spin freezing at similar temperatures as the heat capacity anomalies.
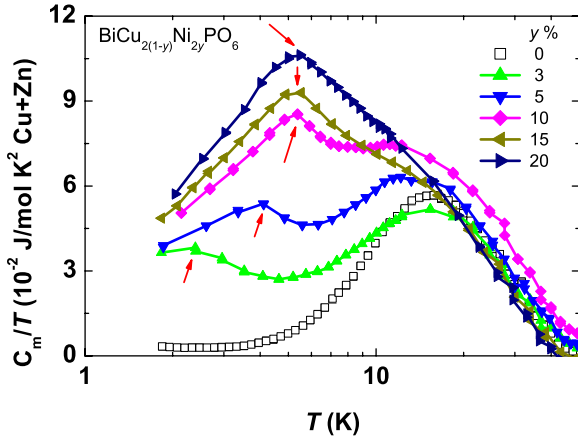
Figure 8. Magnetic specific heat divided by temperature $C_m(T)/T$ versus T for $BiCu_{2(1-y)}Ni_{2y}PO_6$, ($0 \leqslant y \leqslant 0.2$), in the range 1.8–50 K (plotted on a semi-log scale). Anomalies are seen (arrow marks) which might be associated with magnetic freezing.

4.4. Ca/Pb-doped BiCu$_2$PO$_6$

The replacement of Ca^{2+}/Pb^{2+} in place of Bi^{3+} should generate holes. The χ of hole-doped samples $Bi_{1-z}(Pb/Ca)_zCu_2PO_6$ ($0 \leqslant z \leqslant 0.15$) are shown in figure 9(a). The χ increases with doping concentration (z) and no anomalies were found at low-T, in contrast with Zn/Ni-doped samples. Specific heat data are also consistent with this, as shown in the inset of figure 9. There is no change in the position of broad maximum with doping. To obtain the Curie constant of Ca-doped samples, we again plotted $\chi_{imp}^{corr}T$ as a function of T in figure 9(b). For clarity, we have not shown the data of Pb-doped samples in figure 9(b). The effective Curie constant per per cent of doped Ca/Pb amounts to less than one-fourth of that due to an $S = \frac{1}{2}$ moment for each hole, which is even smaller than the value obtained for Zn-doped samples. This might be expected since Pb or Ca substitution at the Bi site does not alter the ladder geometry, but is rather expected to dope holes. It is not known what type of spin state these holes (which are evidently localized) form due to hybridization of the Pb/Ca orbitals with the neighboring orbitals. The Curie term might then be partly due to oxygen non-stoichiometry and partly due to the localized holes, apart from any extrinsic effects.

5. Conclusion

In summary, we have given a detailed account of the preparation and properties of Ni-, Zn-, Pb-, and Ca-doped $BiCu_2PO_6$. While Zn has complete solid solubility, Ni can be substituted up to a concentration of about 20% and Ca up to about 15%. The effective magnetic coordination number for $BiCu_2PO_6$ was found to be about 7 from an analysis of the susceptibility data. The heat capacity for $BiZn_2PO_6$ is well fitted in the T-range 2–100 K by a superposition of two Debye functions, with Debye temperatures of about 180 and 450 K. The magnetic entropy of $BiCu_2PO_6$ is quenched at low temperatures, presumably due to frustration. Both, Ni and Zn doping in $BiCu_2PO_6$ are found to give rise to
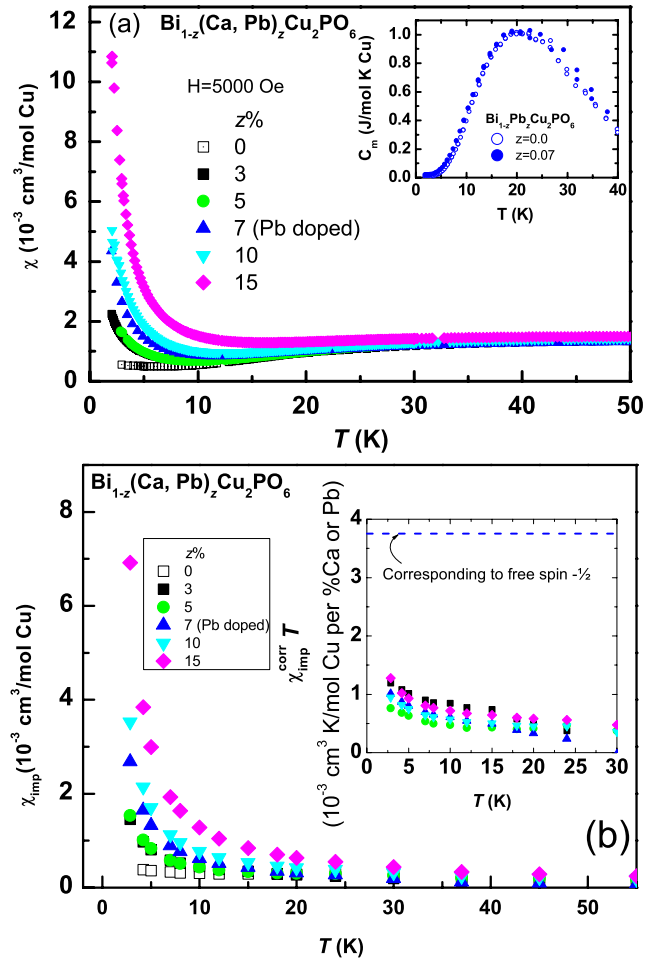
Figure 9. (a) The $\chi(T)$ of $Bi_{1-z}(Ca/Pb)_zCu_2PO_6$ ($0 \leqslant z \leqslant 0.15$) is shown. The inset shows $C_m(T)$ for pure and Pb-doped ($z = 0.07$) samples. (b) A plot of the non-spin-gap part of the susceptibility χ_{imp} for $Bi_{1-z}(Ca/Pb)_zCu_2PO_6$ (i.e., only from impurity-induced effects and from extrinsic impurities) is shown as a function of T. The inset shows $\chi_{imp}^{corr}T$ per per cent Ca as a function of T.

static, disordered magnetism at low temperatures. While clear anomalies were found in the temperature dependence of magnetic susceptibility and magnetic heat capacity of the Ni-doped samples, the Zn-doped samples merely exhibited a deviation from Curie behavior at low temperature, while the heat capacity showed a weak anomaly. The impurity-induced moment is found to be reduced from the $S = 1/2$ value in Zn-doped $BiCu_2PO_6$, which might be due to frustration effects [35]. On the other hand, Ca- and Pb-doped samples gave rise to only weak Curie terms and a nearly unchanged magnetic heat capacity $C_m(T)$, which implies that the magnetic ladders/planes are not disturbed by the doping at the Bi site and any carriers generated localize at low temperatures.

References

[1] Vasil'ev A N, Markina M M and Popova E A 2005 *Low Temp. Phys.* **31** 203
[2] Dagotto E and Rice T M 1996 *Science* **271** 618
[3] Anderson P W 1987 *Science* **235** 1196
[4] Sachdev S 2000 *Science* **288** 475
[5] Mahajan A V, Alloul H, Collin G and Marucco J F 1994 *Phys. Rev. Lett.* **72** 3100
[6] Bobroff J, MacFarlane W A, Alloul H, Mendels P, Blanchard N, Collin G and Marucco J-F 1999 *Phys. Rev. Lett.* **83** 4381
[7] Julien M-H, Fehér T, Horvatic M, Berthier C, Bakharev O N, Ségransan P, Collin G and Marucco J-F 2000 *Phys. Rev. Lett.* **84** 3422
[8] Mendels P, Bobroff J, Collin G, Alloul H, Gabay M, Marucco J-F, Blanchard N and Grenier B 1999 *Europhys. Lett.* **46** 678
    Ouazi S, Bobroff J, Alloul H, Le Tacon M, Blanchard N, Collin G, Julien M H, Horvatic M and Berthier C 2006 *Phys. Rev. Lett.* **96** 127005
[9] Tedoldi F, Santachiara R and Horvatic M 1999 *Phys. Rev. Lett.* **83** 412
    Das J, Mahajan A V, Bobroff J, Alloul H, Alet F and Sorensen E S 2004 *Phys. Rev.* B **69** 144404
[10] Ohsugi S, Tokunaga Y, Ishida K, Kitaoka Y, Azuma M, Fujishiro Y and Takano M 1999 *Phys. Rev.* B **60** 4181
[11] Martins G B, Laukamp M, Riera J and Dagotto E 1997 *Phys. Rev. Lett.* **78** 3563
    Laukamp M, Martins G B, Gazza C, Malvezzi A L, Dagotto E, Hansen P M, Lopez A C and Riera J 1998 *Phys. Rev.* B **57** 10755
[12] Larkin M I, Fudamoto Y, Gat I M, Kinkhabwala A, Kojima K M, Luke G M, Merrin J, Nachumi B, Uemura Y J, Azuma M, Saito T and Takano M 2000 *Phys. Rev. Lett.* **85** 1982
[13] Azuma M, Fujishiro Y, Takano M, Nohara M and Takagi H 1997 *Phys. Rev.* B **55** R8658
[14] Johnston D C 1996 *Phys. Rev.* B **54** 13009
[15] Johnston D C, Kremer R K, Troyer M, Wang X, Klümper A, Budko S L, Panchula A F and Canfield P C 2000 *Phys. Rev.* B **61** 9558
[16] Chakraborty A *et al* 1989 *Phys. Rev.* B **40** 5296
    Xiao G *et al* 1990 *Phys. Rev.* B **42** 240
    Uchinokura K *et al* 1995 *Physica* B **205** 234
[17] Olariu A, Mendels P, Bert F, Duc F, Trombe J C, de Vries M A and Harrison A 2008 *Phys. Rev. Lett.* **100** 087202
    Gregor K and Motrunich O I 2008 *Phys. Rev.* B **77** 184423
[18] Dommange S, Mambrini M, Normand B and Mila F 2003 *Phys. Rev.* B **68** 224416
[19] Okamoto Y, Nohara M, Aruga-Katori H and Takagi H 2007 *Phys. Rev. Lett.* **99** 137207
[20] Koteswararao B, Salunke S, Mahajan A V, Dasgupta I and Bobroff J 2007 *Phys. Rev.* B **76** 052402
[21] Mentré O, Ketatni E M, Colmont M, Huvé M, Abraham F and Petricek V 2006 *J. Am.Chem. Soc.* **128** 10857
[22] Bobroff J *et al* 2009 *Phys. Rev. Lett.* **103** 047201
[23] http://www.ill.fr/dif/Soft/fp/index.html
[24] Abraham F, Ketatni M, Mairesse G and Mernari B 1994 *Euro. J. Solid. Inorg. Chem.* **31** 313
    Ketatni E M, Mernari B, Abraham F and Mentre O 2000 *J. Solid. Chem.* **153** 48
[25] Troyer M, Tsunetsugu H and Würtz D 1994 *Phys. Rev.* B **50** 13515
[26] Selwood P W 1956 *Magnetochemistry* (New York: Interscience)
[27] Alexander L K *et al* unpublished
[28] Johnston D C, Troyer M, Miyahara S, Lidsky D, Ueda K, Azuma M, Hiroi Z, Takano M, Isobe M, Ueda Y, Korotin M A, Anisimov V I, Mahajan A V and Miller L L 2000 arXiv:cond-mat/0001147
[29] Singh Y and Johnston D C 2007 *Phys. Rev.* B **76** 012407
[30] Adroja D T *et al* unpublished
[31] Capriotti L, Scalapino D J and White S R 2004 *Phys. Rev. Lett.* **93** 177004
[32] see, for example, Gopal E S R 1966 *Specific Heats at Low Temperatures* (New York: Plenum)
[33] Johnston D C, Kremer R K, Troyer M, Wang X, Klümper A, Budko S L, Panchula A F and Canfield P C 2000 *Phys. Rev.* B **61** 9558
[34] Sandvik A W, Dagotto E and Scalapino D J 1997 *Phys. Rev.* B **56** 11701
[35] Normand B and Mila F 2002 *Phys. Rev.* B **65** 104411
[36] Grenier B *et al* 1998 *Phys. Rev.* B **58** 8202
    Simonet V *et al* 2006 *Eur. Phys. J.* B **53** 155